DIAGNOSTICS

A digital microfluidic system for serological immunoassays in remote settings

Alphonsus H. C. Ng,[1,2*†] Ryan Fobel,[1,2*] Christian Fobel,[1,2*] Julian Lamanna,[1,2*] Darius G. Rackus,[1,2*] Aimee Summers,[3] Christopher Dixon,[1] Michael D. M. Dryden,[1] Charis Lam,[1] Man Ho,[1,2] Nooman S. Mufti,[2,4] Victor Lee,[2] Mohd Afiq Mohd Asri,[2] Edward A. Sykes,[1,2] M. Dean Chamberlain,[1,2] Rachael Joseph,[5] Maurice Ope,[5] Heather M. Scobie,[6] Alaine Knipes,[3] Paul A. Rota,[7] Nina Marano,[8] Paul M. Chege,[9] Mary Njuguna,[9] Rosemary Nzunza,[9] Ngina Kisangau,[9] John Kiogora,[10] Michael Karuingi,[10] John Wagacha Burton,[11] Peter Borus,[12] Eugene Lam,[3‡] Aaron R. Wheeler[1,2,4§]

Serosurveys are useful for assessing population susceptibility to vaccine-preventable disease outbreaks. Although at-risk populations in remote areas could benefit from this type of information, they face several logistical barriers to implementation, such as lack of access to centralized laboratories, cold storage, and transport of samples. We describe a potential solution: a compact and portable, field-deployable, point-of-care system relying on digital microfluidics that can rapidly test a small volume of capillary blood for disease-specific antibodies. This system uses inexpensive, inkjet-printed digital microfluidic cartridges together with an integrated instrument to perform enzyme-linked immunosorbent assays (ELISAs). We performed a field validation of the system's analytical performance at Kakuma refugee camp, a remote setting in northwestern Kenya, where we tested children aged 9 to 59 months and caregivers for measles and rubella immunoglobulin G (IgG). The IgG assays were determined to have sensitivities of 86% [95% confidence interval (CI), 79 to 91% (measles)] and 81% [95% CI, 73 to 88% (rubella)] and specificities of 80% [95% CI, 49 to 94% (measles)] and 91% [95% CI, 76 to 97% (rubella)] (measles, *n* = 140; rubella, *n* = 135) compared with reference tests (measles IgG and rubella IgG ELISAs from Siemens Enzygnost) conducted in a centralized laboratory. These results demonstrate a potential role for this point-of-care system in global serological surveillance, particularly in remote areas with limited access to centralized laboratories.

INTRODUCTION

Vaccine-preventable diseases (VPDs) such as measles and rubella continue to infect susceptible populations around the world, resulting in an estimated 134,200 deaths from measles (*1*) and 100,000 children born with birth defects from congenital rubella syndrome (*2*) each year. Populations displaced by humanitarian emergencies are especially vulnerable to VPDs because of low vaccination coverage, overcrowding, malnutrition, and reduced access to health care (*3*). Accordingly, the World Health Organization (WHO) recognizes displaced populations, including refugees, as a high-risk group for outbreaks from diseases like measles. The Global Measles and Rubella Strategic Plan 2016–2020 (*4*) includes using effective tools to monitor disease transmission and immunization program efforts and developing rapid, cost-effective tools for vaccination and testing toward measles and rubella elimination.

Population assessments of the seroprevalence of protective immunoglobulin G (IgG) antibodies (known as "serological surveys" or "serosurveys") can help to assess the population's risk for outbreaks and evaluate the efficacy of immunization program efforts (*5*). This strategy is particularly useful for antigenically stable pathogens such as measles and rubella, for which there is a correlation between the presence of serum IgG and immunity (*6*), indicative of previous vaccination or infection (*7*). In economically developed regions with strong health systems, serosurveillance (often using serosurveys) is an important part of VPD surveillance systems (*8*, *9*). Unfortunately, serosurveys are underused in remote settings because of the costs and logistical challenges associated with collecting blood and transporting serum samples to centralized laboratories (*10*). As a result, most coverage survey evaluations in these settings rely on vaccination records or a mother's recall of her child's vaccination history. These methods are often inadequate for demonstrating the true population immunity, which can also be affected by suboptimal vaccine effectiveness related to improper storage conditions, or by host factors like malnutrition (*5*, *7*, *11*).

The work described here fits into the long history of the development of microfluidic or "lab-on-a-chip" technologies that can enable rapid, laboratory-quality immunoassays at the point of need (*12*–*14*). To reduce costs for these kinds of tests, most researchers have focused on either improving the performance of paper-based lateral flow

[1]Department of Chemistry, University of Toronto, 80 St. George Street, Toronto, Ontario M5S 3H6, Canada. [2]Donnelly Centre for Cellular and Biomolecular Research, University of Toronto, 160 College Street, Toronto, Ontario M5S 3E1, Canada. [3]Division of Global Health Protection, Centers for Disease Control and Prevention, 1600 Clifton Road Northeast, Atlanta, GA 30329, USA. [4]Institute of Biomaterials and Biomedical Engineering, University of Toronto, 164 College Street, Toronto, Ontario M5S 3G9, Canada. [5]Centers for Disease Control and Prevention, Kenya Medical Research Institute (KEMRI) Complex, P.O. Box 606-00621, Mbagathi Road Off Mbagathi Way, Village Market, Nairobi, Kenya. [6]Global Immunization Division, Centers for Disease Control and Prevention, Atlanta, GA 30329, USA. [7]Division of Viral Diseases, Centers for Disease Control and Prevention, Atlanta, GA 30329, USA. [8]Division of Global Migration and Quarantine, Centers for Disease Control and Prevention, Atlanta, GA 30329, USA. [9]Kenya Field Epidemiology and Laboratory Training Program, Ministry of Health, P.O. Box 30016–00100, Afya House, Cathedral Road, Nairobi, Kenya. [10]International Rescue Committee, P.O. Box 62727, Galana Plaza, 4th Floor Galana Road, Kilimani, Nairobi, Kenya. [11]Office of the United Nations High Commissioner for Refugees, P.O. Box 43801-00100, Lynwood Court, Off Waiyaki Way, Westland, Nairobi, Kenya. [12]KEMRI, P.O. Box 54840-00200, Off Mbagathi Road, Nairobi, Kenya.
*These authors contributed equally to this work.
†Present address: Division of Chemistry and Chemical Engineering, California Institute of Technology, 1200 East California Boulevard, Pasadena, CA 91125, USA.
‡Present address: Division of Health Emergencies and Communicable Diseases, World Health Organization Regional Office for Europe, UN City, Marmorvej 51, DK-2100 Copenhagen Ø, Denmark.
§Corresponding author. Email: aaron.wheeler@utoronto.ca

assays (LFAs) (*15*–*18*) or developing inexpensive methods for manufacturing high-performance microchannels and related techniques (*19*–*21*). Both rely on fluid flow through a precise sequence of prepatterned and dedicated device features, which guide the movement of reagents through the many steps required to carry out an assay [such as enrichment (*22*), mixing (*23*), reacting (*24*), incubating (*25*), washing (*26*), and detecting (*27*)]. These methods hold great promise for use in diagnostic confirmation of suspected illnesses, but the nature of these devices limits them to use with one patient sample at a time, which poses challenges for serosurveys that typically require large sample sizes (*28*).

An alternative to fluid flow in paper- or microchannel-based devices is digital microfluidics (DMF), in which fluids are manipulated as discrete droplets by electrostatic forces on an array of insulated electrodes (*29*). DMF systems actuate droplets through the application of electrical potentials on a generic array of insulated electrodes—a format that enables software-reconfigurable, concurrent droplet operations including merging, mixing, splitting, and metering from reservoirs (*30*, *31*). Thus, DMF devices are capable of handling multiple samples in parallel and carrying out an assortment of assay protocols with the same chip design, making it a promising platform to explore for application to serosurveillance.

To our knowledge, DMF devices have not been used outside of a laboratory. Moreover, we are unaware of any previous reports on the use of non-LFA–based microfluidic tests in a refugee camp. Here, we describe the development of low-cost DMF cartridges, portable control systems, and parallel assays for the detection of measles virus– and rubella virus–specific IgG in pinprick samples of whole blood. To evaluate the performance of our system as a potential serosurveillance tool, we performed field testing in Kakuma, a refugee camp located in remote northwestern Kenya. The field test results were compared with reference tests [measles IgG and rubella IgG enzyme-linked immunosorbent assays (ELISAs) from Siemens Enzygnost] performed by the national laboratory at Kenya Medical Research Institute (KEMRI), which is accredited by the WHO Global Measles-Rubella Laboratory Network (*32*). The results demonstrate a potential role for DMF in serosurveillance, particularly in areas where centralized laboratories are unavailable.

RESULTS

Cartridge, assay, and control system development and testing

DMF cartridges, assays, and control systems were developed and optimized for fieldwork. The DMF cartridge (Fig. 1A) comprises top and bottom plates that sandwich droplets of sample and reagents. The bottom plate consists of an array of metal electrodes coated by an insulator and a hydrophobic layer. For most cartridges, an inexpensive commercial inkjet printer was used to print conductive silver ink onto a flexible substrate, which served as the bottom plate of the device (Fig. 1B), resulting in a final cost of U.S. $6.00 per cartridge. Each cartridge was assigned unique batch/device identifiers (Fig. 1C), which were encoded within quick response (QR) codes [two-dimensional (2D), scannable labels], and subjected to a two-stage quality control process to ensure robust field performance. Briefly, in the first stage, [quality control stage 1 (QC-1), illustrated in fig. S1], 6 of 30 bottom plates were discarded during manufacture. In the second stage (QC-2, illustrated in fig. S2), about 25% of bottom plates were not used for assays (eventually sourced to a particular batch of dielectric deposition that was apparently substandard).

For DMF measles and rubella ELISAs, paramagnetic particles coated with viral antigens capture measles IgG or rubella IgG from the sample (Fig. 1D) and are then processed for chemiluminescent detection. Besides the rubella virus–coated particles [which were donated from a commercial source (*33*)], measles virus–functionalized particles and all other assay reagents were formulated and prepared in-house for compatibility with DMF. After loading samples onto a cartridge, the liquid handling steps moved particles and droplets through the nine sequential steps of each assay, culminating in movement of droplets to a detection zone where chemiluminescence correlating to bound IgG was measured (Fig. 1E). At various stages of the assay, activation of a magnetic lens (*34*) underneath the device allowed separation of particles from a supernatant droplet (for example, panel 3 of Fig. 1E). Assays were typically performed with four samples tested in parallel ("fourplex") in a process that required 35 min.

A new instrument measuring 25 cm × 20 cm × 28 cm was developed to perform the DMF assays, dubbed the Measles-Rubella Box (MR Box) (Fig. 2A). Weighing 4 kg and operating from a 12-V laptop power supply, the MR Box is portable for use in the field. The MR Box includes a pogo pin–based DMF cartridge interface (Fig. 2B) and contains a PMT and environmental sensors that are necessary for running microfluidic ELISAs (Fig. 2C). Components of the MR Box were selected to minimize cost, with many formed in-house using inexpensive rapid prototyping tools (for example, 3D printing and laser cutting); the fully assembled instrument costs less than $2500 (table S1). The MR Box represents a substantial upgrade with several key advances relative to heavier and bulkier prototype systems such as those described previously (*33*, *34*). Key advances that are unique to the MR Box are listed in Fig. 1D. Briefly, hardware improvements include (i) an open-source DropBot 3.0 control system (http://microfluidics.utoronto.ca/dropbot/) with a fully integrated high-voltage amplifier and a signal generator (fig. S3); (ii) a servo motor–controlled, rotating magnetic lens with compact form factor for magnetic particle separations (fig. S4); (iii) an integrated, open-source DStat potentiostat (http://microfluidics.utoronto.ca/dstat) for precise control of chemiluminescence measurements (fig. S5); and (iv) a new optical train for high-efficiency collection of chemiluminescent signal, which allows the PMT to be operated at a distance from the DMF cartridge (fig. S6). The software improvements include (v) droplet routing and autorouting path generation (fig. S7); (vi) user-editable metadata fields for storing device, patient, assay identification, as well as time, temperature, and humidity measurements (fig. S8); (vii) click-and-drag webcam device alignment (fig. S9); and (viii) protocol step annotations with user-defined instruction dialogs (fig. S10). A connectivity diagram (fig. S11) illustrates how these features were assembled into the integrated instrument.

The MR Box was evaluated for assay performance in the laboratory at the University of Toronto. Calibration curves for both assays are shown in Fig. 3A. Limits of detection (LODs) and limits of quantitation (LOQs) were 0.14 and 0.55 mIU ml^{-1} for measles IgG and 0.15 and 0.20 IU mL^{-1} for rubella IgG, below the thresholds of protective immunity for measles (*35*) and rubella (*36*). In blinded testing of commercially available serum panels in the laboratory (Fig. 3B), the DMF-ELISAs discriminated between measles IgG-positive and IgG-negative samples from a seroconversion panel (n = 8) with 100% sensitivity [95% confidence interval (CI), 46 to 100%] and 100% specificity (95% CI, 31 to 100%), as compared with results supplied by the vendor. Likewise, the rubella assay tested on a serum panel (n = 20) performed similarly, with 100% sensitivity (95% CI, 78 to 100%)

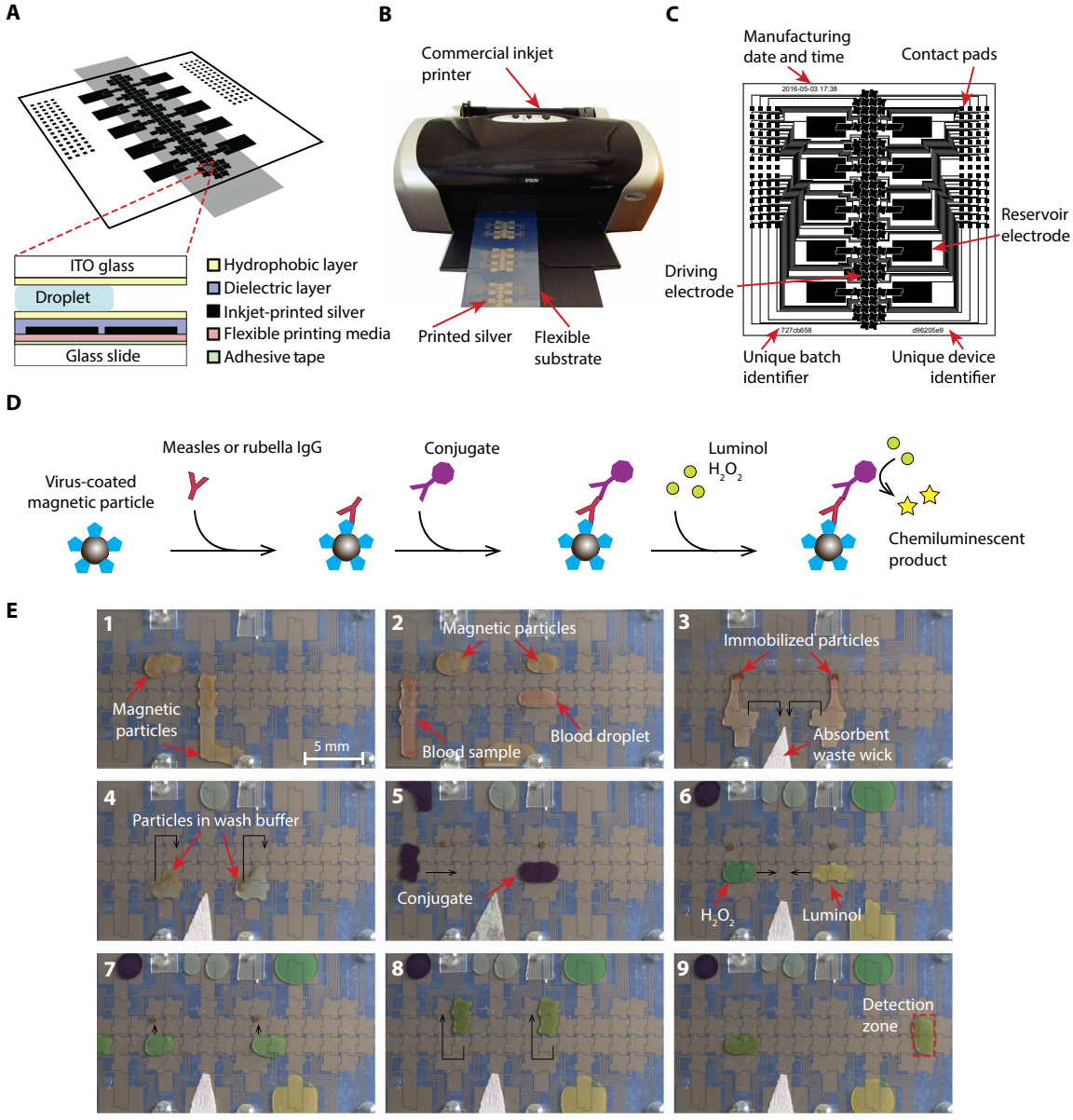

Fig. 1. Digital microfluidic cartridge and ELISA used for measles and rubella testing. (**A**) Isometric-view schematic of the DMF top and bottom plates assembled to form a cartridge. Inset: Cross-section image (not to scale) of a complete device bearing inkjet-printed electrodes (black) coated with dielectric (purple) and hydrophobic (yellow) layers. The flexible printing media (peach) substrate is affixed to a glass slide via double-sided adhesive tape (green). ITO, indium tin oxide. (**B**) Photograph of silver DMF electrodes printed on a flexible substrate using a commercial inkjet printer. (**C**) Top-view schematic of the DMF device with 92 driving electrodes and 10 reservoir electrodes. (**D**) Cartoon schematic of measles and rubella ELISAs. Paramagnetic particles coated with measles or rubella virus antigens are incubated with sample. Anti-measles or anti-rubella IgG (red) binds to the particles. Particles are washed and then incubated with anti-human IgG–horseradish peroxidase conjugate (purple). The particles are washed again and then exposed to a mixture of luminol and H_2O_2 (yellow-green). Enzymatic turnover of the product generates a chemiluminescent product (yellow). (**E**) Photographs of two assays performed in parallel (that is, "twoplex") on a DMF cartridge (dyes are added to enhance droplet visibility; black arrows indicate the direction of droplet movement). (1) Droplets of particle suspension are dispensed; (2) blood samples are dispensed and merged with the particles; (3) particles are immobilized by activating the magnetic lens, and supernatant droplets are removed to an absorbent wick; (4) particles are washed in wash buffer (blue); (5) antibody conjugate (purple) is dispensed and incubated with the particles; (6) after further wash steps, droplets of luminol (yellow) and H_2O_2 (green) are dispensed, mixed, and (7) split; (8) particles are incubated with luminol and H_2O_2; and (9) particles are moved to the detection zone.

and 100% specificity (95% CI, 20 to 100%), as compared with results supplied by the vendor.

Field trial in Kakuma refugee camp

Four MR Boxes were transported as carry-on luggage to Kakuma refugee camp in Kenya for field testing in 23 May to 3 June 2016, in conjunction with a national MR vaccination campaign, which occurred in 16 to 24 May 2016. Table 1 describes the demographics for 144 subjects enrolled in the study: A cohort of 77 caregivers provided blood at the time of enrollment during the vaccination campaign, and 67 children provided blood ~2 weeks after MR vaccination. The cohorts of caregivers and children had median ages of 32 years

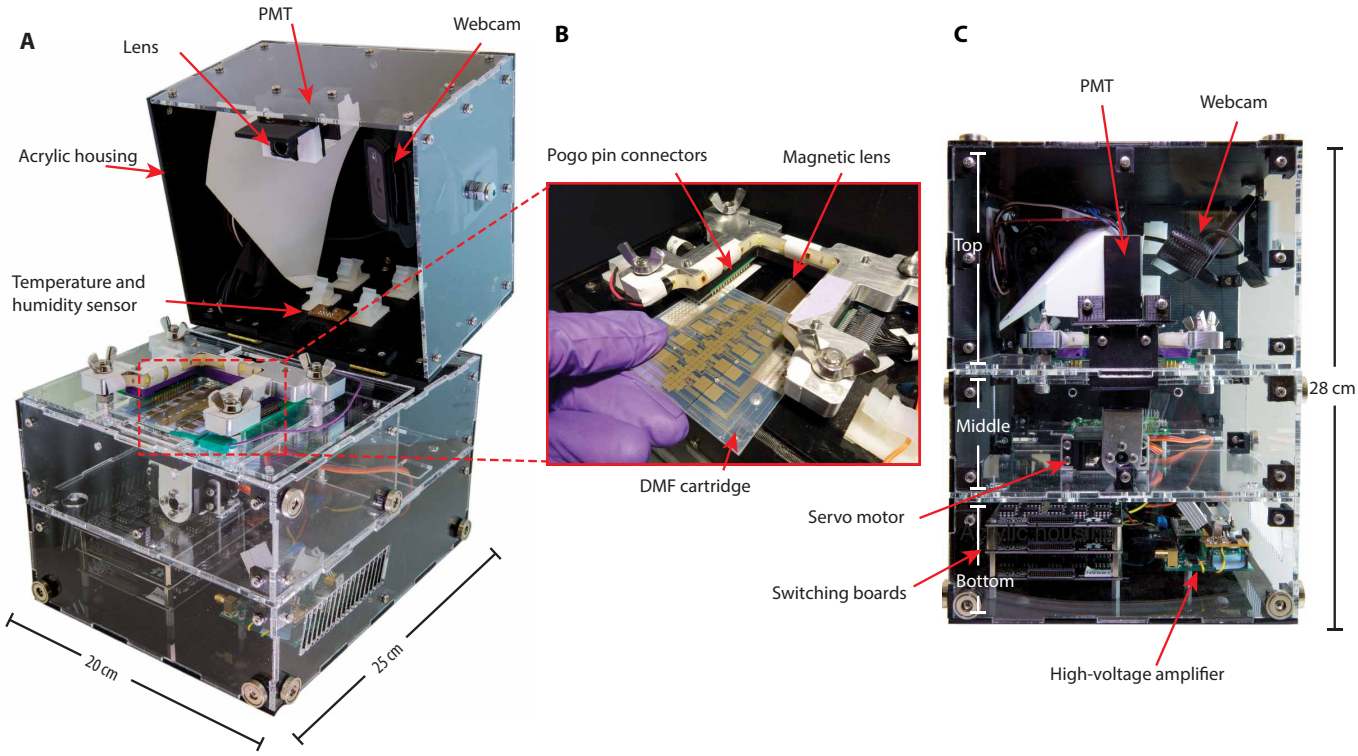

D

	Feature	Effect
Hardware	Integrated high-voltage source	Eliminates bulky external amplifier
	Servo-operated magnet	Immobilizes magnetic particles
	DStat for PMT control	Powers and collects signal from the PMT and integrates with the control software
	Photomultiplier tube and lenses	Collects and records light from chemiluminescent reaction
Software	Droplet routing	Reduces the number of steps in a protocol
	Experiment metadata fields	Stores patient identifier, assay being performed, and layout of assays
	Webcam video correction	"Click-and-drag" adjustment of video feed to match DMF cartridge map
	Step labels	Identifies portions of the protocol for easier management

Fig. 2. Portable MR Box. (**A**) Photograph of the MR Box with transparent sides showing the photomultiplier tube (PMT), lens, webcam, and temperature and humidity sensors. The acrylic housing has a footprint of 25 cm × 20 cm. (**B**) Photograph showing detail of a DMF device being inserted into the MR Box interface. The DMF device sits atop a motorized magnetic lens and interfaces with the control system via pogo pin connectors. (**C**) Photograph (front view; transparent panels) of the MR Box showing the PMT, webcam, servo motor, switching boards, and high-voltage amplifier. With the lid closed, the MR Box measures 28 cm tall. (**D**) Table of innovations that are new to the MR Box hardware (see figs. S3 to S6) and software (see figs. S7 to S10), developed in preparation for the field tests.

(range, 20 to 60) and 20 months (range, 9 to 56), respectively. Whole-blood samples were evaluated on-site using the MR Boxes, during which time the temperatures and humidities recorded during each test ranged from 22° to 28°C and 34 to 57% (fig. S12). Sera were prepared from the same subjects and shipped to KEMRI in Nairobi to be used for reference tests (Siemens Enzygnost ELISAs). According to the reference test results from all samples, measles antibody seroprevalence was 79% among children and 100% among caretakers, whereas rubella seroprevalence was 37 and 100% among those respective populations. Four measles samples and nine rubella samples were found to be in the "equivocal" range of the reference tests; these samples were considered indeterminate and were excluded from further analysis.

Figure 4 shows a comparison of the whole-blood samples evaluated on-site using the new MR Box and prepared sera from the same participants tested using reference tests. Using an empirically defined threshold from receiver operating characteristic (ROC) curve analysis, the MR Box measles assay had a sensitivity of 86% (95% CI, 79 to 91%), a specificity of 80% (95% CI, 49 to 94%), and an overall agreement of 86% (95% CI, 79 to 91%) (n = 140) (Fig. 4A). Similarly, the MR Box rubella assay had a sensitivity of 81% (95% CI, 73 to 88%), a specificity of 91% (95% CI, 76 to 97%), and overall

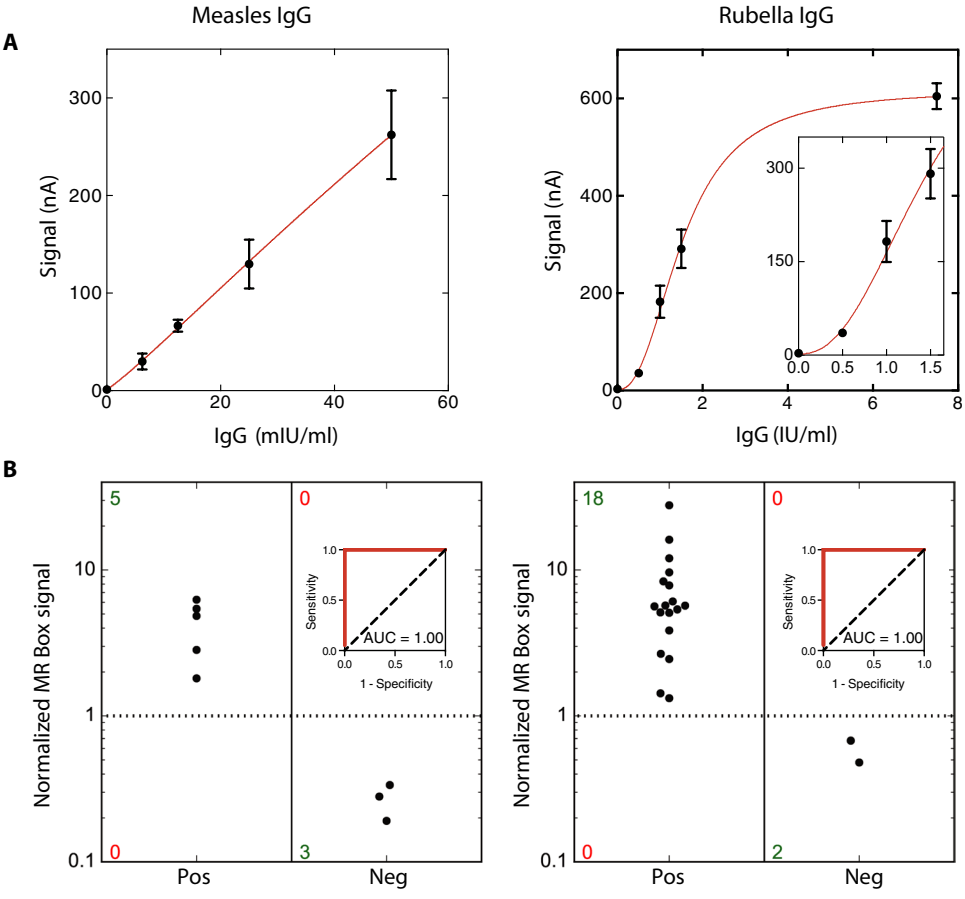

Fig. 3. MR Box assay development and optimization in the laboratory. (**A**) Calibration curves generated from measurements of standards (filled circles) of measles IgG (left) and rubella IgG (right; inset: four lowest concentrations); error bars represent ±1 SD, $n = 4$ per condition. The coefficient of variance (CV) was <20% for each of the 10 conditions evaluated, except for the measles IgG (6.35 mIU/ml) measurement, which had CV of 27.5%. Curves were fitted (red lines) using a four-parameter logistic equation (measles, $R^2 = 0.9998$; rubella, $R^2 = 0.9991$) (**B**) Vertical scatterplots of serum panels tested in the laboratory for measles IgG, $n = 8$ (left) and rubella IgG, $n = 20$ (right). Green and red numbers in the scatterplots represent the number of samples correctly and incorrectly categorized by the MR Box, respectively. The inset plots show ROC curves for MR Box assays (red lines) and random guesses (dashed lines). The area under the curve (AUC) is reported in each plot.

agreement of 84% (95% CI, 76 to 90%) ($n = 135$) (Fig. 4B). Using the MR Box, measles seroprevalence was 70% for children and 91% for caregivers, and rubella seroprevalence was 31 and 90%, respectively.

DISCUSSION

Testing for serological surveillance is typically performed using microtiter plate immunoassays in centralized laboratories (*37*). These assays are intended for measurements using serum and require trained personnel (such as phlebotomists), access to temperature-controlled supply chain, and specialized instrumentation. Collection of dried blood spot (DBS) samples can solve the temperature-controlled supply chain challenge when shipping to a centralized laboratory (*38*), but DBS samples are not universally accepted as equivalent to conventional venous blood draw samples (*10*). For remote populations in settings with limited transportation infrastructure, the use of DBS samples does not solve the problem of long wait times between sample collection and results. We propose that portable tests like the DMF-based MR Box system described here may provide a potential solution to this problem.

Unlike other forms of miniaturized liquid-handling technology (*39*), to our knowledge, DMF had not been used outside the research laboratory before this study. Critical innovations were necessary to move from a bulky laboratory-bound prototype system subject to intermittent performance challenges (*33*, *34*) to a lightweight, inexpensive point-of-care system with reliable performance suitable for fieldwork. One such innovation was the development of low-cost inkjet-printed cartridges, which were assembled by a team of students at a cost of $1.50 per assay (four assays per cartridge). The cost can be reduced by an order of magnitude by using roll-coating techniques (*40*), and further reductions should be possible in the future if manufacturing at larger scale in an industrial setting. Cartridge reliability has also been a concern in previous work, which led us to develop a robust quality control regimen that allowed reliable running of hundreds of assays in the field without access to the typical suite of tools used to troubleshoot assay performance in an academic laboratory.

Another critical development was the new instrument reported here, the MR Box. The previously reported portable DMF control systems (*41*–*43*) have substantially reduced capabilities relative to the instruments that are used in the laboratory, such as a limited number of channels/electrodes and/or detectors with limited sensitivity. In contrast, the MR Box is a fully functional portable control system, capable of robustly completing the thousands of droplet "move," "dispense," "mix," "separate," "resuspend," "wash," and "split" steps necessary to run hundreds of personalized assays in a short period of time. The MR Box combines all the electronic, mechanical, and software components in a single unit with small size that can easily be deployed to remote settings while maintaining reliable performance. Note that although the data reported here were generated by experts (members of an academic research laboratory) working under mild conditions, the improvements in the MR Box are intended as a first step toward making the system straightforward for use by nonexperts under uncontrolled environmental conditions.

In laboratory tests in Toronto before the field trial, we observed 100% agreement between MR Box results and conventional ELISA results for commercial panels of serum samples. This performance is similar to that of other portable tests in the market—for example, the SD Bioline Rubella IgG LFA (Alere) has a manufacturer-reported sensitivity/specificity of 99%/92% (according to the product insert) determined against ELISA. To our knowledge, there are no commercially available portable diagnostic tests for measles IgG, but there

Table 1. Characteristics of field study participants in Kakuma refugee camp, Kenya.

Characteristic	No.	%
Caregivers (n = 77)		
Age (years)		
<25	12	17
25–29	19	25
30–34	17	22
≥35	29	41
Ethnicity		
Sudanese	30	39
Somali	24	31
Ethiopian	12	16
Others	11	14
Children (n = 67)	No.	%
Age (months)		
9–11	15	22
12–23	22	33
24–35	12	18
36–47	10	15
48–59	8	12
Ethnicity		
Somali	33	49
Sudanese	20	30
Ethiopian	9	13
Others	5	8
Time of sample collection after vaccination (days), median (range)	14 (12–23)	

are reports indicating that similar tests are under development (*44*, *45*). For example, a measles IgM LFA has a reported sensitivity/specificity of 91%/94% for serum samples validated against ELISA in a laboratory setting (*45*).

MR Box assay results collected in the field at the Kakuma refugee camp had reduced overall agreement (86 and 84% for measles and rubella, respectively) with laboratory results compared to tests conducted in the laboratory. Similar observations of diminished performance in field trials relative to that determined in the laboratory have been described previously (*46*). There are multiple potential reasons for this effect. First, potential interferants in whole blood were not accounted for in the assay optimization stage because a panel of characterized whole-blood samples were not available at that time. This may have resulted in diminished assay performance in the field (*47*); for example, false positives may arise from hemoglobin interference with luminol (*48*). Second, the tests being compared in this analysis differed substantially in both sample type and assay format. Specifically, the portable test evaluated whole blood with minimum sample handling before analysis, whereas the reference ELISA test evaluated samples that were processed to serum, frozen, shipped, stored, and then thawed before analysis. Likewise, the portable assay relied on magnetic particles in small droplets of sample with high-binding surface area–to–sample volume ratio, whereas the well-plate format of the reference test has a low-binding surface area–to–sample volume ratio. There are a number of confounding factors that might explain discordant results for tests as dissimilar as these, including analyte losses during processing, differing amounts of nonspecific adsorption, varied affinities for the different antibodies used, and differences in sample-constituent degradation rates (each of which might result in false positives or false negatives, depending on which test is biased in what direction). Third, the microtiter plate–based ELISA used as a reference test in our evaluation is an imperfect reference to the gold-standard assay for measles and rubella immunity, which is the plaque reduction neutralization test (PRNT) (*49*). PRNT assays, which require more technical expertise and specialized equipment than standard ELISAs (*50*), were not available for this study, but future calibration of the MR Box system performance directly to PRNT test results may prove useful for further improving the MR Box performance.

In this first field trial of the MR Box, the sensitivity and specificity were imperfect, and future research and fieldwork will continue to improve performance characteristics. However, even with the current performance profile, use of the MR Box may still be considered valuable for use in settings like refugee camps, where immediate availability of seroprevalence results for decision-making around vaccination strategy is critical. A recent modeling study of the use of seroprevalence results to trigger vaccination campaigns demonstrated an associated reduction in measles morbidity from reducing vaccination response time from 6 to 1 month after survey (*51*), suggesting that rapid test technologies like DMF-ELISA would be potentially beneficial for routine programmatic use. Several statistical methods exist for adjusting seroprevalence observed by the nonreference laboratory tests relative to reference tests (*52*). One option is to continue to evaluate a small subset of samples measured by the MR Box using a laboratory reference test to empirically derive field sensitivity and specificity for adjustment each time (*53*, *54*). Ideally, if future field tests of sensitivity and specificity of the MR Box are consistent across different populations, the Rogan-Gladen correction can be used to generate an unbiased estimate of seroprevalance from the portable test results (*55*). Complex statistical models are also available for mitigating bias of testing methods in estimating seroprevalance (*52*). These methods have the advantage of accounting for uncertainty in the adjustment, which could be a factor if actions based on serosurvey results are triggered by crossing a certain seroprevalence threshold.

Finally, we note that in comparison to alternate strategies that might be envisioned for remote testing such as LFAs, the DMF technology described here brings a number of unique practical advantages. Patient samples under such conditions are often collected at an irregular rate, and the on-site MR-Box test described here can adapt to different combinations of rubella (R) and measles (M) tests performed on samples from two to four patients in each cartridge, as needed (for example, 4-R, 3-R/1-M, 2-R/2-M, 1-R/3-M, and 4-M). In the future, throughput per cartridge could be increased, perhaps using thin-film transistor-based DMF devices with thousands of electrodes (*56*). Increases in sample throughput should be accompanied by an increase in the number of assay types used on the same cartridge, for example, adding IgM assays for diagnosis or DMF-based assays for other conditions such as malaria (*57*) or bacterial infections (*58*, *59*). In this manner, the user would have the flexibility to conduct many assays on one sample or to conduct a single assay on

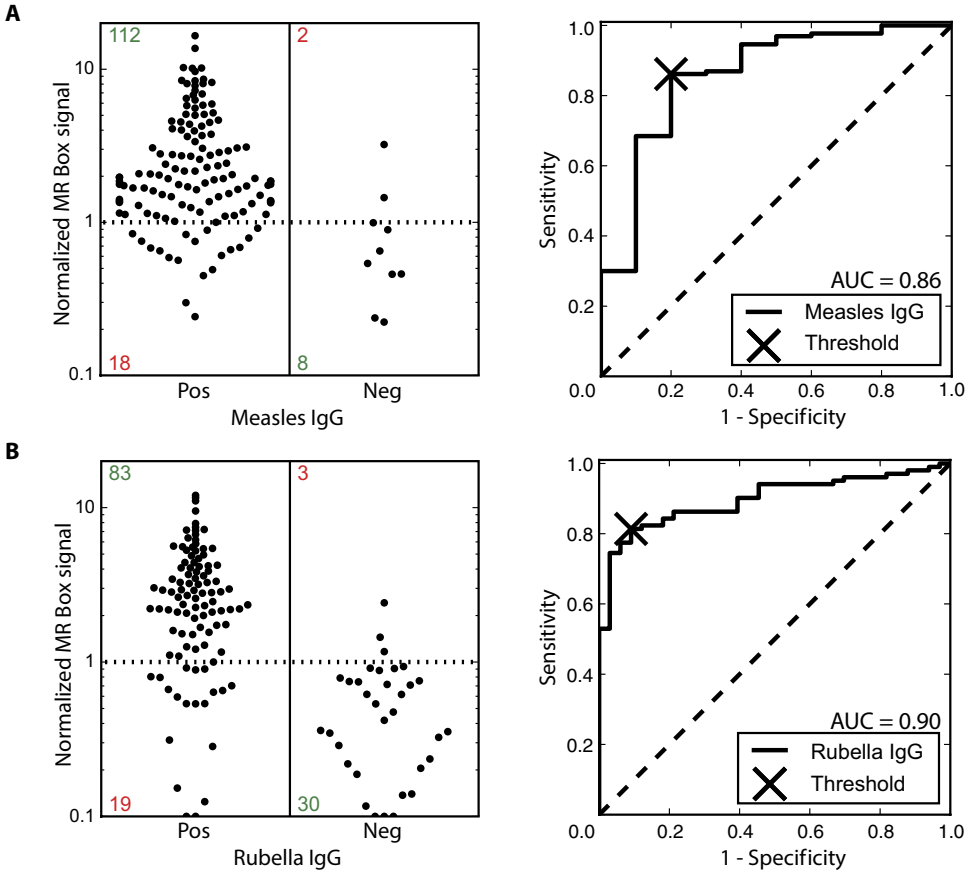

Fig. 4. MR Box field trial in Kakuma refugee camp, Kenya. (**A**) Vertical scatterplot (left) of MR Box signals for samples determined to be positive (Pos) or negative (Neg) for anti-measles IgG by reference tests (n = 140). ROC curve (right) with AUC of 0.86 and threshold (X) selected for sensitivity of 86% (95% CI, 79 to 91%), specificity of 80% (95% CI, 44 to 97%), and overall agreement of 86% (95% CI, 79 to 91%) are shown. (**B**) Vertical scatterplot (left) of MR Box signals for samples determined to be positive or negative for anti-rubella IgG by reference tests (n = 135). ROC curve (right) with AUC of 0.90 and threshold (X) selected for sensitivity of 81% (95% CI, 72 to 88%), specificity of 91% (95% CI, 75 to 98%), and overall agreement of 84% (95% CI, 76 to 90%) are shown. Green and red numbers in the scatterplots represent the number of samples correctly and incorrectly categorized by the MR Box, respectively.

many samples (or any permutation thereof) depending on the need. Finally, the flexibility of these types of configurations should allow for systems in the field to receive remote updates, revisions, and new assay protocols wirelessly based on optimization and development performed elsewhere.

In summary, the system described here represents a new and potentially useful tool for conducting timely measles and rubella serosurveillance in remote settings. We propose that the flexibility inherent to DMF combined with low-cost open-source instruments and cartridges will be attractive for a wide range of global health applications that require portable analyses. The platform's potential impact and reach could be heightened when coupled with different detection modalities and sensors (*60*–*62*), bringing the combination of integrated sample processing with high-performance diagnostics into the field.

METHODS

Study design

The objective of this research was to evaluate the performance of the MR Box DMF-ELISA and to assess its potential role in carrying out serological immunoassays in remote settings. The MR Box and DMF-ELISAs were used to test samples collected from subjects residing in the Kakuma refugee camp in northwestern Kenya during a national MR vaccination campaign. Two cohorts were recruited from the population residing in Kakuma: children 9 to 59 months of age participating in the vaccination campaign (or receiving routine immunizations) and their caregivers; caregivers provided informed consent for themselves and their children. The target numbers for each cohort was 75 (a total of 150). Sample size was calculated assuming a sensitivity and specificity of 95% with a precision of ±5% for the DMF-ELISA test, 52 positive and 52 negative samples by the reference test were determined to be required. Assuming that 75% of the children would be IgG-negative and 75% of the mothers or caregivers would be IgG-positive by the reference test, we calculated that 75 participants would be required from each group to have a greater than 75% probability of obtaining a sample of 52 or more, based on the binomial distribution.

At enrollment, caregivers were asked their and their children's age, sex, ethnicity, and whether they were currently pregnant. Informed consent was obtained from all research participants. Local health care workers collected all adult samples (during each child's vaccination visit) and child samples (12 to 23 days post-vaccination). Venipuncture blood samples (10 ml) were collected from all subjects. Finger-prick samples (200 to 250 μl) were collected in BD Microtainer K2 EDTA tubes (BD). Aliquots (250 μl) were immediately isolated from venipuncture samples from children for analysis by MR Box; the remainder of these samples and the entirety of samples collected from adults were allowed to clot by standing for 15 to 30 min at room temperature and centrifuged at 2000*g* for 10 min, and a supernatant (serum) was collected in a separate tube. Serum samples were frozen on-site and shipped to KEMRI at the end of the field study (19 days after commencement). Serum samples were stored at 2° to 8°C until analysis and tested at KEMRI (using a plate reader) using the Siemens Enzygnost measles IgG ELISA and Siemens Enzygnost rubella IgG ELISA kits (Behringwerke AG), as per manufacturer's instructions. Testing was double-blinded between on-site and reference tests. This study was approved by the Scientific Steering and Ethical Review Committees of the KEMRI.

Samples to be analyzed by MR Box were collected either by aliquotting directly from venous blood draw (for children) or by finger prick (for adults; 200 to 250 μl) into BD Microtainer tubes with K2 EDTA. The rate of sample collection was variable, and not every sample could be processed on the day it was collected; those that were not tested immediately were stored at 4°C until evaluation. Each day,

a team of researchers from Toronto residing outside the camp traveled into the camp, where they operated four MR Boxes in a small room in the medical clinic operated by the International Rescue Committee. This room was equipped with AC power and had intermittent air conditioning.

Materials and reagents

Unless otherwise specified, reagents were purchased from Sigma-Aldrich, and electronic components were purchased from Digi-Key. Deionized water (DI H_2O) with a resistivity of >18 megohm·cm was used to prepare all aqueous solutions.

DMF-ELISA reagents were prepared in advance of the field trial and formulated as follows. Wash buffer was Dulbecco's phosphate-buffered saline (PBS) supplemented with 0.1% (w/v) ethylenediamine tetrakis(ethoxylate-block-propoxylate) tetrol (Tetronic 90R4, BASF Corp.). Sample diluent was PBS supplemented with 4% (w/v) bovine serum albumin (BSA) and 0.1% (w/v) Tetronic 90R4. Blocking diluent was Superblock tris-buffered saline (Thermo Fisher Scientific) supplemented with 0.1% (w/v) Tetronic 90R4. Conjugate solution was horseradish peroxidase–conjugated goat polyclonal anti-human IgG (21 ng/ml) in blocking diluent. Stable peroxide (H_2O_2) and luminol/enhancer solutions were adapted from SuperSignal ELISA Femto kits (Thermo Fisher Scientific), each supplemented with 0.05% (w/v) Tetronic 90R4. Rubella IgG standards and rubella virus–coated 5.0-μm-diameter paramagnetic particles were adapted from Abbott Architect rubella IgG assay kits, each supplemented with 0.1% (w/v) Tetronic 90R4. Measles IgG standard (WHO Third International Standard, UK National Institute for Biological Standards and Control) was supplemented with 0.1% (w/v) Tetronic 90R4.

Edmonston strain measles virus (catalog #7604, Meridian Life Science Inc.) was immobilized on amine-terminated 3.07-μm-diameter paramagnetic particles (Bangs Laboratories) via disuccinimidyl tartrate (DST) (Toronto Research Chemicals). Briefly, a 50-μl aliquot of particles (2.59×10^9 particles/ml) was washed twice in 400 μl DI H_2O, twice in 400 μl of 0.1 M sodium bicarbonate with 0.01 % (w/v) Tween 20, and twice in 400 μl of 0.1 M sodium bicarbonate. The particles were then resuspended in 100 μl of 0.1 M sodium bicarbonate with measles antigen (40 fg per particle) and DST (3.29 pg per particle, dissolved in dimethyl sulfoxide) and incubated at room temperature for 2 hours with rotation. The particles were then washed four times in 400 μl of PBS containing 1% (w/v) BSA and 0.05% (w/v) Tween 20 and then blocked by incubating in 100-μl Superblock with rotation at 4°C overnight. Finally, the particles were washed four times in 1 ml of DMF blocking diluent and were resuspended to a final concentration of 9×10^8 particles/ml in DMF blocking diluent supplemented with 20% sucrose for long-term (>1 month) storage. Before use, both measles virus– and rubella virus–functionalized particles were washed twice in 1 ml of blocking diluent and resuspended in blocking diluent at 9×10^8 (measles) or 1.5×10^8 (rubella) particles/ml.

DMF cartridge design and manufacture

Each DMF cartridge was assembled from (Ia) an inkjet-printed bottom plate or (Ib) a photolithographically defined bottom plate and (II) an ITO-coated glass top plate (Fig. 1). Both types of bottom plates (Ia,b) featured 92 roughly square interdigitated driving electrodes (2.8 mm × 2.8 mm), 10 reservoir electrodes (10 mm × 6.7 mm), and 10 dispensing electrodes (5.2 mm × 2.4 mm). For inkjet-printed bottom plates (Ia), an Epson C88+ inkjet printer (Seiko Epson Corporation) was used to deposit Metalon JS-B25P silver nanoparticle ink onto Novele IJ-220 substrates (NovaCentrix), as described previously (*40*). After printing, devices were diced and affixed to glass slides (S.I. Howard Glass Co. Inc.) with double-sided adhesive tape (3M Company). Photolithographically defined bottom plates (Ib) were formed from Cr-coated glass slides (Telic Company), as described elsewhere (*34*). After patterning, all bottom plates were coated with a ~7-μm-thick layer of parylene C (Specialty Coating Systems) by chemical vapor deposition and a ~50-nm-thick layer of FluoroPel PFC 1101V (Cytonix LLC) by spin-coating. For (II), top plates were fabricated by spin-coating a ~50-nm-thick layer of FluoroPel PFC 1101V onto ITO-coated glass slides (75 mm × 25 mm) (Delta Technologies).

Each cartridge was completed by adhering a top-plate/bottom-plate pair via two layers of double-sided adhesive tape (3M Company), forming an interplate spacer of ~180 μm, and was reinforced with ultraviolet light-curable glue (Bondic). Triangular (~5-mm height × ~10-mm base) absorbent tissues (Kimberly-Clark) were inserted between the top and bottom plates for use as waste reservoirs, and an adhesive label with a QR code was affixed to the back of every cartridge. More than 1000 cartridges were formed and used for method optimization and testing; 450 cartridges (including 300 with inkjet-printed and 150 photolithographically defined bottom plates) were used in the field trial.

DMF cartridge quality control

Each batch of printed bottom-plate substrates (~30) was subjected to a custom QC-1 test (i) after printing, (ii) after coating with parylene, and (iii) after coating with FluoroPel. In each QC-1 test, a top plate was temporarily mounted to the substrate, and a custom MR Box capacitance scan was applied to identify devices with cut or broken traces (fig. S1), which were discarded. Scan outcomes were matched with batch/device identifiers; these data were used to optimize the fabrication process. Immediately before use, all cartridges were subjected to QC-2. Briefly, the QR code was scanned by a laptop controlling an MR Box, and two droplets (4 to 6 μl each) of wash buffer were loaded and moved around the device, recording the velocity over each electrode (fig. S2) in the cartridge's metadata file. No differences in failure rate or overall device performance were observed between cartridges formed with printed or photolithographically defined bottom plates.

DMF control system (MR Box) design, manufacture, and operation

Each MR Box weighed 4 kg, measured 25 cm × 20 cm × 28 cm ($l \times w \times h$) (Fig. 2), and was enclosed in a black polymethyl methacrylate (PMMA) plastic (Plastic World) housing, with pieces formed using a 40-W H-Series Desktop CO_2 Laser (Full Spectrum Laser). External faces of the housing, as well as internal wiring ports within the box, were covered with 3M 3903 Black Vinyl Duct Tape (Uline) and removable black, 3-mm PMMA cladding via MM-B-16 mounts (K&J Magnetics Inc.) to render the system light-tight. Mechanical hardware (for example, 3-mm machine screws, nuts, washers, and hinges) was purchased from McMaster-Carr, and custom fixtures and brackets were 3D-printed in polylactic acid (PLA) plastic using an Ultimaker 2 3D printer (Ultimaker). MR Box components are described below and are summarized in fig. S11 and table S1. More than 15 MR Box prototypes were formed and used during method development and optimization; four were used in the field trial.

The top section of each MR Box was mounted in a hinged lid. A Hamamatsu H10721-01 PMT (Hamamatsu Corp.) was mounted on a 3D-printed PLA bracket affixed to the front panel of the lid. Two aspherical

condenser lenses (ACL1210U-A, Thorlabs Inc.) were mounted in a 3D-printed PLA housing, positioned immediately below the PMT (fig. S6). A camera [LifeCam Studio 1080p (Microsoft Corporation) or HD Pro Webcam C920 (Logitech)] was affixed to the inside of the lid at ~60° relative to the cartridge surface. A panel of 24 light-emitting diodes (LEDs) (White LED 24 SMD 3528 Panel, Amazon.ca) was affixed to the lid and combined with white cardstock to diffuse and reflect light. A custom 1.5-cm × 3-cm printed circuit board bearing a temperature/humidity sensor (HIH6030-021-001, Honeywell) was mounted on the inside of the lid.

The middle section of each MR Box measured was divided into two compartments (front and rear) by a PMMA divider. The front featured the DMF cartridge manifold, which comprised a custom printed circuit board with 120 pogo pin connectors mounted on a custom aluminum bracket (10 cm × 14.5 cm × 1 cm; University of Toronto Chemistry Machine Shop) via a 3D-printed PLA spacer. The manifold was spring-mounted (adjusted with wingnuts) on four rails (Type 316 stainless steel shoulder screws $^{1}/_{4}$″-20 thread). A panel of 11 LEDs (Susay Waterproof LED Light Strip; Amazon.ca) was affixed to the aluminum manifold. A magnetic lens module, which featured a BZ084 neodymium permanent magnet (3″ × 1/2″ × 1/4″, 0.33-T surface field; K&J Magnetics Inc.) modified with a magnetic lens as described previously (*33*, *34*), machined from AISI 1080 steel (University of Toronto Chemistry Machine Shop), was positioned below the cartridge manifold. The magnet and lens were housed in a 3D-printed PLA casing attached to a TowerPro MG995 servo motor via a tilt bracket (McMaster-Carr). When rotated to 83° with respect to the bottom of the instrument, the magnet was "activated"; when rotated to 10°, the magnet was "deactivated" (fig. S4). The rear compartment housed a DStat [described in detail elsewhere (*63*), freely available open-source at http://microfluidics.utoronto.ca/dstat, used to measure the current produced by the PMT (fig. S5)].

The bottom section of each MR Box contained custom electronic circuits for (i) driving droplet movement (DropBot 3.0, freely available open-source at http://microfluidics.utoronto.ca/dropbot/), (ii) controlling the position of the magnet, and (iii) controlling the states of the LEDs and temperature and humidity sensors. Power was supplied by a 65-W power brick (100 to 240 VAC input/12 VDC, 5-A output) and a 5V step-down voltage regulator (Pololu). All components interfaced to a laptop computer via an Anker four-port USB 3.0 hub (Amazon.ca). The DropBot electronics comprised a high-voltage AC signal source capable of generating bipolar waveforms up to 140 V_{rms} at 100 Hz to 10 kHz and switching boards with optical isolator switches. Two of the four MR Box instruments used in the field [relying on a version of DropBot described previously (*64*)] were operated using a low-voltage 0- to 20-V peak-to-peak AC signal source coupled with an external PZ700 amplifier (TREK Inc.). The other two MR Box instruments used in the field relied on DropBot 3.0 (reported here for the first time), which features a fully integrated high-voltage AC signal source comprising a step-up boost converter based on the MAX1771 chip (Maxim Integrated), a square wave driver built with an NCP5304 chip (ON Semiconductor), and a pair of IRF740B power MOSFETs (Vishay Intertechnology) in totem pole configuration. The resulting square wave was passed through a first-order, high-pass filter to remove the DC component, thus creating a bipolar signal (fig. S3). No differences in performance were observed between the two types of instruments.

Each MR Box was controlled using a new version (2.0) of open-source MicroDrop (*64*) and DStat-interface (*63*) programs, and a collection of custom MicroDrop 2.0 plugins written in Python (http://python.org), including "metadata_plugin" to record cartridge and sample identification (as well as data collected) (fig. S8), "dropbot-dx-accessories-plugin" to control the magnet, lighting, and interface with the DStat for reading the PMT current, "user_prompt_plugin" to prompt users at specific steps in the protocol (fig. S10), "device-quality-control-plugin" to probe cartridges for broken and shorted connections (fig. S1), "step_label_plugin" to assign labels to each step of a MicroDrop protocol, and "droplet-planning-plugin" to automatically route droplet paths and simplify protocol composition (fig. S7). Source code for MicroDrop 2.0 and all plugins is freely available at https://github.com/wheeler-microfluidics.

Microfluidic operations and DMF-ELISA

The minimum volume used was a "double-unit" 2.4-μl droplet that covered two driving electrodes. Fluidic operations included move, dispense, mix, separate, resuspend, wash, and split. For move, DropBot applied 90 to 110 V_{rms}, 10-kHz square waves between the top-plate counter electrode and sequential driving electrodes on the bottom plate. For dispense, a reservoir electrode and four adjacent driving electrodes were actuated for 8 s, after which the two middle electrodes were turned off for 9 s, allowing the fluid to pinch into a double-unit droplet. For mix, two droplets were merged, and then the pooled droplet was moved across 11 electrodes in a circular pattern. For separate, the magnet was activated under a droplet containing paramagnetic particles for 24 s, whereas the supernatant was driven away (typically to waste). For resuspend, the magnet was deactivated under immobilized particles on the device surface, and a droplet was moved onto the particles and then mixed for 20 s. For wash, particles were separated from an origin droplet, resuspended in a destination droplet, and then separated again. For split, electrodes on either side of a merged droplet (formed from two double-unit droplets) were actuated, whereas the central electrodes were turned off for 9 s, allowing the fluid to pinch into two double-unit droplets.

Before analysis, 2 μl of sample was diluted off-chip (1:20 for whole blood or 1:40 for serum) in sample diluent, and 8 μl of this diluted sample was loaded into a reservoir on a cartridge. The cartridge was inserted into the MR Box, where the camera feed was aligned to the device design (fig. S9), and then the steps were managed via MicroDrop (fig. S10). DMF-ELISAs were performed in nine steps (Fig. 1E): (1) A double-unit droplet of particle suspension was dispensed. (2) A double-unit droplet of sample was dispensed and mixed with the particles for 7 min. (3) The particles were separated, and the supernatant was taken to waste. (4) The particles were washed sequentially in two double-unit droplets of wash buffer, and the supernatants were moved to waste. (5) A double-unit droplet of conjugate solution was dispensed and used to resuspend the particles and then mixed for 5 min. (6) The particles were washed sequentially in four double-unit droplets of wash buffer, and the supernatants were moved to waste. (7) One double-unit droplet each of luminol and H_2O_2 solutions was dispensed and then mixed for 30 s and finally split. (8) One of the split droplets was used to resuspend the particles, which were then further mixed for 2 min (rubella) or 8 min (measles). The other split droplet was used for another assay run in parallel or was moved to waste. (9) The droplet bearing resuspended particles was moved to the detection zone, and chemiluminescence was measured by the PMT (10 s collected at 60 Hz, recording the mean of the final 8 s). After each test, cartridges were disposed as biohazardous waste.

In practice, four assays were typically run in parallel (that is, fourplex), which required 35 min to complete. Unique reagents were loaded individually [for example, the samples in step (2)], and common reagents were loaded once and then dispensed multiple times (for example, the magnetic particle suspension in step 1). In each fourplex assay, the PMT recorded five measurements. The first measurement was a background, collected before step (1) with no droplet in the detection zone; the remainder was sequential measurements of processed samples in step (9). Once each day, a calibrator solution [1:40 dilution of rubella IgG (10 IU ml^{-1}) in serum or measles IgG (250 mIU ml^{-1}) in serum] was measured by each MR Box. Before sample analysis, each sample and calibrator measurement were corrected by background subtraction and then reported as the ratio between the sample and calibrator signals to normalize for variations between MR Boxes.

The nine-step MR Box procedure described above was determined after thousands of assays and run on various prototypes of the MR Box in the laboratory. After optimization, dilutions of IgG serum calibrators in sample diluent were plotted as a function of concentration and fit with four-parameter logistic curves. The LODs and LOQs were defined as the concentrations (from the fitted functions) correlating to the average blank signal plus 3 or 10 times the SD of the blank signal, respectively (Fig. 3A). The assays were applied to testing a measles IgG seroconversion panel (Biomex GmbH) and a mixed titer rubella IgG serum panel (PTR201, SeraCare). ROC curves were obtained by comparing MR Box signals to the results of reference standard tests using interpretations provided by the manufacturer (Fig. 3B).

Statistical analysis

Normalized MR Box signals were extracted and compiled into Microsoft Excel (Microsoft Corporation) using Python packages SciPy, Numpy (*65*), IPython (*66*), and Pandas (*67*). GraphPad Prism 6 (GraphPad Software Inc.) and Stata 14 (StataCorp LP) were used for ROC curve analysis. Samples classified as equivocal by reference standard ELISAs were removed, and the remaining samples were plotted in ROC curves comparing MR Box results to reference test results. Thresholds giving optimal combinations of clinical sensitivity and specificity were selected from ROC curves (Fig. 4). Sensitivities, specificities, and Wilson 95% CIs were calculated using Stata v14 and Microsoft Excel 2013.

SUPPLEMENTARY MATERIALS

www.sciencetranslationalmedicine.org/cgi/content/full/10/438/eaar6076/DC1
Fig. S1. Quality control procedure 1.
Fig. S2. Quality control procedure 2.
Fig. S3. Integrated control system.
Fig. S4. Magnetic separation.
Fig. S5. PMT control.
Fig. S6. Detection.
Fig. S7. Droplet programming.
Fig. S8. Assay metadata.
Fig. S9. Device alignment.
Fig. S10. Program interface.
Fig. S11. MR Box connectivity diagram.
Fig. S12. Temperature and humidity.
Table S1. MR Box bill of materials.

REFERENCES AND NOTES

1. "Measles Fact Sheet," (WHO Publication, 2016; www.who.int/mediacentre/factsheets/fs286/en/).
2. "Rubella Fact Sheet," (WHO Publication, 2016; www.who.int/mediacentre/factsheets/fs367/en/).
3. E. Lam, A. McCarthy, M. Brennan, Vaccine-preventable diseases in humanitarian emergencies among refugee and internally-displaced populations. *Hum. Vaccin. Immunother.* **11**, 2627–2636 (2015).
4. "Global measles and rubella strategic plan: 2012–2020" (WHO Publication, 2016); http://apps.who.int/iris/bitstream/10665/44855/1/9789241503396_eng.pdf.
5. C. J. E. Metcalf, J. Farrar, F. T. Cutts, N. E. Basta, A. L. Graham, J. Lessler, N. M. Ferguson, D. S. Burke, B. T. Grenfell, Use of serological surveys to generate key insights into the changing global landscape of infectious disease. *Lancet* **388**, 728–730 (2016).
6. W. J. Moss, S. Scott, "WHO Immunological Basis for Immunization Series Module 7: Measles" (WHO Publication, 2009); http://apps.who.int/iris/bitstream/10665/44038/1/9789241597555_eng.pdf.
7. K. T. Hayford, H. M. Al-Emran, W. J. Moss, M. S. Shomik, D. Bishai, O. S. Levine, Validation of an anti-measles virus-specific IgG assay with oral fluid samples for immunization surveillance in Bangladesh. *J. Virol. Methods* **193**, 512–518 (2013).
8. K. Osborne, J. Weinberg, E. Miller, The European Sero-Epidemiology Network. *Eurosurveillance* **2**, 167 (1997).
9. H. Gidding, Australia's national serosurveillance program. *N. S. W. Public Health Bull.* **14**, 90–93 (2003).
10. F. T. Cutts, M. Hanson, Seroepidemiology: An underused tool for designing and monitoring vaccination programmes in low- and middle-income countries. *Trop. Med. Int. Health* **21**, 1086–1098 (2016).
11. K. T. Hayford, M. S. Shomik, H. M. Al-Emran, W. J. Moss, D. Bishai, O. S. Levine, Measles vaccination coverage estimates from surveys, clinic records, and immune markers in oral fluid and blood: A population-based cross-sectional study. *BMC Public Health* **13**, 1211 (2013).
12. D. Mabey, R. W. Peeling, A. Ustianowski, M. D. Perkins, Tropical infectious diseases: Diagnostics for the developing world. *Nat. Rev. Microbiol.* **2**, 231–240 (2004).
13. E. Fu, P. Yager, P. N. Floriano, N. Christodoulides, J. T. McDevitt, Perspective on diagnostics for global health. *IEEE Pulse* **2**, 40–50 (2011).
14. W. Jung, J. Han, J.-W. Choi, C. H. Ahn, Point-of-care testing (POCT) diagnostic systems using microfluidic lab-on-a-chip technologies. *Microelectron. Eng.* **132**, 46–57 (2015).
15. A. W. Martinez, S. T. Phillips, M. J. Butte, G. M. Whitesides, Patterned paper as a platform for inexpensive, low-volume, portable bioassays. *Angew. Chem. Int. Ed.* **46**, 1318–1320 (2007).
16. N. R. Pollock, J. P. Rolland, S. Kumar, P. D. Beattie, S. Jain, F. Noubary, V. L. Wong, R. A. Pohlmann, U. S. Ryan, G. M. Whitesides, A paper-based multiplexed transaminase test for low-cost, point-of-care liver function testing. *Sci. Transl. Med.* **4**, 152ra129 (2012).
17. E. Fu, T. Liang, P. Spicar-Mihalic, J. Houghtaling, S. Ramachandran, P. Yager, Two-dimensional paper network format that enables simple multistep assays for use in low-resource settings in the context of malaria antigen detection. *Anal. Chem.* **84**, 4574–4579 (2012).
18. M. S. Akram, R. Daly, F. da Cruz Vasconcellos, A. K. Yetisen, I. Hutchings, E. A. H. Hall, Applications of paper-based diagnostics, in *Lab-on-a-Chip Devices and Micro-Total Analysis Systems: A Practical Guide*, J. Castillo-León, W. E. Svendsen, Eds. (Springer International Publishing, 2015), pp. 161–195.
19. T. Laksanasopin, T. W. Guo, S. Nayak, A. A. Sridhara, S. Xie, O. O. Olowookere, P. Cadinu, F. Meng, N. H. Chee, J. Kim, C. D. Chin, E. Munyazesa, P. Mugwaneza, A. J. Rai, V. Mugisha, A. R. Castro, D. Steinmiller, V. Linder, J. E. Justman, S. Nsanzimana, S. K. Sia, A smartphone dongle for diagnosis of infectious diseases at the point of care. *Sci. Transl. Med.* **7**, 273re271 (2015).
20. C. D. Chin, T. Laksanasopin, Y. K. Cheung, D. Steinmiller, V. Linder, H. Parsa, J. Wang, H. Moore, R. Rouse, G. Umviligihozo, E. Karita, L. Mwambarangwe, S. L. Braunstein, J. van de Wijgert, R. Sahabo, J. E. Justman, W. El-Sadr, S. K. Sia, Microfluidics-based diagnostics of infectious diseases in the developing world. *Nat. Med.* **17**, 1015–1019 (2011).
21. C. D. Chin, Y. K. Cheung, T. Laksanasopin, M. M. Modena, S. Y. Chin, A. A. Sridhara, D. Steinmiller, V. Linder, J. Mushingantahe, G. Umviligihozo, E. Karita, L. Mwambarangwe, S. L. Braunstein, J. van de Wijgert, R. Sahabo, J. E. Justman, W. El-Sadr, S. K. Sia, Mobile device for disease diagnosis and data tracking in resource-limited settings. *Clin. Chem.* **59**, 629–640 (2013).
22. A. E. Herr, A. V. Hatch, D. J. Throckmorton, H. M. Tran, J. S. Brennan, W. V. Giannobile, A. K. Singh, Microfluidic immunoassays as rapid saliva-based clinical diagnostics. *Proc. Natl. Acad. Sci. U.S.A.* **104**, 5268–5273 (2007).
23. P. B. Howell Jr., D. R. Mott, S. Fertig, C. R. Kaplan, J. P. Golden, E. S. Oran, F. S. Ligler, A microfluidic mixer with grooves placed on the top and bottom of the channel. *Lab Chip* **5**, 524–530 (2005).
24. C. J. Easley, J. M. Karlinsey, J. M. Bienvenue, L. A. Legendre, M. G. Roper, S. H. Feldman, M. A. Hughes, E. L. Hewlett, T. J. Merkel, J. P. Ferrance, J. P. Landers, A fully integrated microfluidic genetic analysis system with sample-in–answer-out capability. *Proc. Natl. Acad. Sci. U.S.A.* **103**, 19272–19277 (2006).
25. R. Gottheil, N. Baur, H. Becker, G. Link, D. Maier, N. Schneiderhan-Marra, M. Stelzle, Moving the solid phase: A platform technology for cartridge based sandwich immunoassays. *Biomed. Microdevices* **16**, 163–172 (2014).
26. Q. Ramadan, M. A. M. Gijs, Simultaneous sample washing and concentration using a "trapping-and-releasing" mechanism of magnetic beads on a microfluidic chip. *Analyst* **136**, 1157–1166 (2011).

27. F. B. Myers, L. P. Lee, Innovations in optical microfluidic technologies for point-of-care diagnostics. *Lab Chip* **8**, 2015–2031 (2008).
28. "Guidance on conducting serosurveys in support of measles and rubella elimination in the WHO European Region" (WHO Publication, 2013); www.euro.who.int/en/health-topics/communicable-diseases/measles-and-rubella/publications/2013/guidance-on-conducting-serosurveys-in-support-of-measles-and-rubella-elimination-in-the-who-european-region-2013.
29. K. Choi, A. H. C. Ng, R. Fobel, A. R. Wheeler, Digital microfluidics. *Annu. Rev. Anal. Chem.* **5**, 413–440 (2012).
30. M. G. Pollack, R. B. Fair, A. D. Shenderov, Electrowetting-based actuation of liquid droplets for microfluidic applications. *Appl. Phys. Lett.* **77**, 1725–1726 (2000).
31. S. K. Cho, H. Moon, C.-J. Kim, Creating, transporting, cutting, and merging liquid droplets by electrowetting-based actuation for digital microfluidic circuits. *J. Microelectromech. Syst.* **12**, 70–80 (2003).
32. M. N. Mulders, P. A. Rota, J. P. Icenogle, K. E. Brown, M. Takeda, G. J. Rey, M. C. Ben Mamou, A. R. Dosseh, C. R. Byabamazima, H. J. Ahmed, S. Pattamadilok, Y. Zhang, M. Gacic-Dobo, P. M. Strebel, J. L. Goodson, Global Measles and Rubella Laboratory Network support for elimination goals, 2010–2015. *MMWR Morb. Mortal. Wkly. Rep.* **65**, 438–442 (2016).
33. A. H. Ng, M. Lee, K. Choi, A. T. Fischer, J. M. Robinson, A. R. Wheeler, Digital microfluidic platform for the detection of rubella infection and immunity: A proof of concept. *Clin. Chem.* **61**, 420–429 (2015).
34. K. Choi, A. H. C. Ng, R. Fobel, D. A. Chang-Yen, L. E. Yarnell, E. L. Pearson, C. M. Oleksak, A. T. Fischer, R. P. Luoma, J. M. Robinson, J. Audet, A. R. Wheeler, Automated digital microfluidic platform for magnetic-particle-based immunoassays with optimization by design of experiments. *Anal. Chem.* **85**, 9638–9646 (2013).
35. M.-S. Lee, D. J. Nokes, Predicting and comparing long-term measles antibody profiles of different immunization policies. *Bull. World Health Organ.* **79**, 615–624 (2001).
36. L. P. Skendzel, Rubella immunity: Defining the level of protective antibody. *Am. J. Clin. Pathol.* **106**, 170–174 (2016).
37. W. Dimech, M. N. Mulders, A 16-year review of seroprevalence studies on measles and rubella. *Vaccine* **34**, 4110–4118 (2016).
38. A. Uzicanin, I. Lubega, M. Nanuynja, S. Mercader, P. Rota, W. Bellini, R. Helfand, Dried blood spots on filter paper as an alternative specimen for measles diagnostics: Detection of measles immunoglobulin M antibody by a commercial enzyme immunoassay. *J. Infect. Dis.* **204** (suppl. 1), S564–S569 (2011).
39. A. A. Kumar, J.W. Hennek, B. S. Smith, S. Kumar, P. Beattie, S. Jain, J. P. Rolland, T. P. Stossel, C. Chunda-Liyoka, G. M. Whitesides, From the bench of the field in low-cost diagnostics: Two case studies. *Angew. Chem. Int. Ed.* **54**, 5836–5853 (2015).
40. C. Dixon, A. H. C. Ng, R. Fobel, M. B. Miltenburg, A. R. Wheeler, An inkjet printed, roll-coated digital microfluidic device for inexpensive, miniaturized diagnostic assays. *Lab Chip* **16**, 4560–4568 (2016).
41. C. Peng, Z. Zhang, C. J. Kim, Y. S. Ju, EWOD (electrowetting on dielectric) digital microfluidics powered by finger actuation. *Lab Chip* **14**, 1117–1122 (2014).
42. M. Yafia, A. Ahmadi, M. Hoorfar, H. Najjaran, Ultra-portable smartphone controlled integrated digital microfluidic system in a 3D-printed modular assembly. *Micromachines* **6**, 1289 (2015).
43. Z. Zeng, K. Zhang, W. Wang, W. Xu, J. Zhou, Portable electrowetting digital microfluidics analysis platform for chemiluminescence sensing. *IEEE Sens. J.* **16**, 4531–4536 (2016).
44. H. Singh, K. Morioka, M. Shimojima, L. Van An, H. Nakajima, A. Hemmi, K. Uchiyama, S. K. Loong, S. AbuBakar, M. Yang, M. Sugamata, A handy field-portable ELISA system for rapid onsite diagnosis of infectious diseases. *Jpn. J. Infect. Dis.* **69**, 435–438 (2016).
45. L. Warrener, R. Slibinskas, K. B. Chua, W. Nigatu, K. E. Brown, K. Sasnauskas, D. Samuel, D. Brown, A point-of-care test for measles diagnosis: Detection of measles-specific IgM antibodies and viral nucleic acid. *Bull. World Health Organ.* **89**, 675–682 (2011).
46. T. M. Kashosi, J. M. Mutuga, D. S. Byadunia, J. K. Mutendela, B. Mulenda, K. Mubagwa, Performance of SD Bioline Malaria Ag Pf/Pan rapid test in the diagnosis of malaria in South-Kivu, DR Congo. *Pan Afr. Med. J.* **27**, 216 (2017).
47. J. Tate, G. Ward, Interferences in immunoassay. *Clin. Biochem. Rev.* **25**, 105–120 (2004).
48. T. Olsson, K. Bergström, A. Thore, A sensitive method for determination of serum hemoglobin based on iso-luminol chemiluminescence. *Clin. Chim. Acta* **122**, 125–133 (1982).
49. B. J. Cohen, D. Doblas, N. Andrews, Comparison of plaque reduction neutralisation test (PRNT) and measles virus-specific IgG ELISA for assessing immunogenicity of measles vaccination. *Vaccine* **26**, 6392–6397 (2008).
50. J. M. Hubschen, S. M. Bork, K. E. Brown, A. Mankertz, S. Santibanez, M. Ben Mamou, M. N. Mulders, C. P. Muller, Challenges of measles and rubella laboratory diagnostic in the era of elimination. *Clin. Microbiol. Infect.* **23**, 511–515 (2017).
51. J. Lessler, C. J. E. Metcalf, F. T. Cutts, B. T. Grenfell, Impact on epidemic measles of vaccination campaigns triggered by disease outbreaks or serosurveys: A modeling study. *PLOS Med.* **13**, e1002144 (2016).
52. F. I. Lewis, P. R. Torgerson, A tutorial in estimating the prevalence of disease in humans and animals in the absence of a gold standard diagnostic. *Emerg. Themes Epidemiol.* **9**, 1742–7622 (2012).
53. A. Tenenbein, A double sampling scheme for estimating from binomial data with misclassifications. *J. Am. Stat. Assoc.* **65**, 1350–1361 (1970).
54. A. Tenenbein, A double sampling scheme for estimating from binomial data with misclassifications: Sample size determination. *Biometrics* **27**, 935–944 (1971).
55. W. J. Rogan, B. Gladen, Estimating prevalence from the results of a screening test. *Am. J. Epidemiol.* **107**, 71–76 (1978).
56. B. Hadwen, G. R. Broder, D. Morganti, A. Jacobs, C. Brown, J. R. Hector, Y. Kubota, H. Morgan, Programmable large area digital microfluidic array with integrated droplet sensing for bioassays. *Lab Chip* **12**, 3305–3313 (2012).
57. D. G. Rackus, R. P. S. de Campos, C. Chan, M. M. Karcz, B. Seale, T. Narahari, C. Dixon, M. D. Chamberlain, A. R. Wheeler, Pre-concentration by liquid intake by paper (P-CLIP): A new technique for large volumes and digital microfluidics. *Lab Chip* **17**, 2272–2280 (2017).
58. R. Sista, Z. Hua, P. Thwar, A. Sudarsan, V. Srinivasan, A. Eckhardt, M. Pollack, V. Pamula, Development of a digital microfluidic platform for point of care testing. *Lab Chip* **8**, 2091–2104 (2008).
59. Z. Hua, J. L. Rouse, A. E. Eckhardt, V. Srinivasan, V. K. Pamula, W. A. Schell, J. L. Benton, T. G. Mitchell, M. G. Pollack, Multiplexed real-time polymerase chain reaction on a digital microfluidic platform. *Anal. Chem.* **82**, 2310–2316 (2010).
60. G. Borghei, E. A. H. Hall, BRET-linked ATP assay with luciferase. *Analyst* **139**, 4185–4192 (2014).
61. R. Griss, A. Schena, L. Reymond, L. Patiny, D. Werner, C. E. Tinberg, D. Baker, K. Johnsson, Bioluminescent sensor proteins for point-of-care therapeutic drug monitoring. *Nat. Chem. Biol.* **10**, 598–603 (2014).
62. K. Pardee, A. A. Green, M. K. Takahashi, D. Braff, G. Lambert, J. W. Lee, T. Ferrante, D. Ma, N. Donghia, M. Fan, N. M. Daringer, I. Bosch, D. M. Dudley, D. H. O'Connor, L. Gehrke, J. J. Collins, Rapid, low-cost detection of Zika virus using programmable biomolecular components. *Cell* **165**, 1255–1266 (2016).
63. M. D. M. Dryden, A. R. Wheeler, DStat: A versatile, open-source potentiostat for electroanalysis and integration. *PLOS ONE* **10**, e0140349 (2015).
64. R. Fobel, C. Fobel, A. R. Wheeler, DropBot: An open-source digital microfluidic control system with precise control of electrostatic driving force and instantaneous drop velocity measurement. *Appl. Phys. Lett.* **102**, 193513 (2013).
65. S. van der Walt, S. C. Colbert, G. Varoquaux, The NumPy array: A structure for efficient numerical computation. *Comput. Sci. Eng.* **13**, 22–30 (2011).
66. F. Pérez, B. E. Granger, IPython: A system for interactive scientific computing. *Comput. Sci. Eng.* **9**, 21–29 (2007).
67. W. McKinney, in *Proceedings of the 9th Python in Science Conference* (2010), pp. 51–56.

Acknowledgments: We thank S. Nayak (Columbia University), K. Hayford (Johns Hopkins University), K. Kain (University of Toronto), R. Campos (University of Toronto), and T. Narahari (University of Toronto) for fruitful discussions. We thank C. Okello and J. Sitati [Centers for Disease Control and Prevention (CDC) Kenya] for assistance with the logistics for the field team; E. Ojwang (International Rescue Committee) for assistance in initial planning and field protocol development; P. Kimani (Office of the United Nations High Commissioner for Refugees) for providing an enabling environment for performing the field tests; R. Nyoka (CDC Kenya) for assistance with data management; K. Wannemuehler (CDC Atlanta) for statistical consultation; and L. Ngo (University of Toronto) for assistance with photography, logistics, and personnel support. The findings and conclusions in this report are those of the authors and do not necessarily represent the official position of the CDC. **Funding:** This work was supported by Stars in Global Health (Grand Challenges Canada), Emergency Response and Recovery Branch (ERRB) Innovation Grant (CDC), Abbott Laboratories, Canada Research Chair Program (Government of Canada) (to A.R.W.), NSERC (Natural Sciences and Engineering Research Council of Canada) E.W.R. Steacie Memorial Fellowship, Queen Elizabeth II Graduate Scholarship in Science and Technology (Government of Ontario) (to D.G.R.), NSERC Postgraduate Scholarship (to M.D.M.D.). **Author contributions:** A.H.C.N., R.F., and A.R.W. conceived the idea and wrote the initial proposal. A.H.C.N., R.F., C.F., M.D.M.D., E.A.S., N.S.M., M.D.C., and M.A.M.A. designed, optimized, and built the portable DMF control systems. A.H.C.N., C.F., C.D., M.H., and V.L. designed, optimized, and manufactured the DMF cartridges. A.H.C.N., J.L., D.G.R., C.D., C.L., and P.A.R. designed, developed, and optimized the DMF assays and collected the DMF laboratory data. E.L., R.J., M.O., A.S., H.M.S., and J.W.B. planned, scouted, and arranged the field tests. E.L., A.S., A.K., J.K., M.K., and N.M. collected and processed blood and serum field samples and coordinated data collection. A.H.C.N., R.F., C.F., and J.L. conducted the DMF field tests. P.B., N.K., P.M.C., M.N., and R.N. coordinated and conducted the reference laboratory tests. A.H.C.N., C.F., R.F., D.G.R., J.L., A.S., and A.R.W. analyzed the field and laboratory data. A.H.C.N., C.F., D.G.R., and A.R.W. prepared and optimized the figures. D.G.R. and A.R.W. wrote the paper with input from the entire team. **Competing interests:** R.F., C.F., and A.R.W. are co-founders of Sci-Bots Inc., which sells a commercial version of the

open-source DropBot system described here. R.F. and A.R.W. are inventors on issued patent U.S. 9,594,056 B2, which covers methods that can be used to fabricate some of the cartridge components described here. A.H.C.N., R.F., M.H., and A.R.W. are inventors on submitted patent application PCT/CA2017/050398, which covers a droplet additive that was included in some of the assays described here. **Data and materials availability:** All reagents needed to run assays can be prepared as described here, other than the rubella virus–modified beads and IgG calibrators, which were a gift from Abbott Laboratories. The open-source hardware systems DropBot 3.0 and DStat 1.0 can be assembled as described here and at http://microfluidics.utoronto.ca/dropbot and http://microfluidics.utoronto.ca/dstat, respectively. The source code for the open-source software system MicroDrop 2.0 is available at https://github.com/wheeler-microfluidics.

Submitted 28 November 2017
Accepted 6 April 2018
Published 25 April 2018
10.1126/scitranslmed.aar6076

Citation: A. H. C. Ng, R. Fobel, C. Fobel, J. Lamanna, D. G. Rackus, A. Summers, C. Dixon, M. D. M. Dryden, C. Lam, M. Ho, N. S. Mufti, V. Lee, M. A. M. Asri, E. A. Sykes, M. D. Chamberlain, R. Joseph, M. Ope, H. M. Scobie, A. Knipes, P. A. Rota, N. Marano, P. M. Chege, M. Njuguna, R. Nzunza, N. Kisangau, J. Kiogora, M. Karuingi, J. W. Burton, P. Borus, E. Lam, A. R. Wheeler, A digital microfluidic system for serological immunoassays in remote settings. *Sci. Transl. Med.* **10**, eaar6076 (2018).

Science Translational Medicine

A digital microfluidic system for serological immunoassays in remote settings

Alphonsus H. C. Ng, Ryan Fobel, Christian Fobel, Julian Lamanna, Darius G. Rackus, Aimee Summers, Christopher Dixon, Michael D. M. Dryden, Charis Lam, Man Ho, Nooman S. Mufti, Victor Lee, Mohd Afiq Mohd Asri, Edward A. Sykes, M. Dean Chamberlain, Rachael Joseph, Maurice Ope, Heather M. Scobie, Alaine Knipes, Paul A. Rota, Nina Marano, Paul M. Chege, Mary Njuguna, Rosemary Nzunza, Ngina Kisangau, John Kiogora, Michael Karuingi, John Wagacha Burton, Peter Borus, Eugene Lam and Aaron R. Wheeler

Sci Transl Med **10**, eaar6076.
DOI: 10.1126/scitranslmed.aar6076

A fluid transition into the field

Many point-of-care diagnostics rely on lateral flow assays or microfluidics; however, these methods generally cannot test multiple samples simultaneously. Ng *et al*. optimized inkjet-printed digital microfluidic (DMF) cartridges and a portable control system to perform serological immunoassays in remote settings. DMF devices use electrostatic forces to mix and separate reagents and samples in small droplets of fluids. The DMF system measured IgG antibodies for measles and rubella from human blood samples obtained from adults and children on-site in a refugee camp in Kenya. Four samples could be tested simultaneously, although DMF IgG detection was less sensitive and specific than laboratory-based ELISA testing of matched serum samples. The emergence of this field-compatible technology brings with it new tools for advancing global health.